DOI: 10.13009/EUCASS2023-650
Aerospace Europe Conference 2023 – 10TH EUCASS – 9TH CEAS

Stability analysis of simplified labyrinth seals model to geometric and flow hypotheses

G. Foschi[⋆†]*, F. Thouverez*[⋆]*, L. Blanc*[⋆]*, G. Fiore*[‡]*, G. Pampolini*[§]*, P. Girard*[¶]
[⋆]*Ecole Centrale de Lyon, Laboratoire de Tribologie et Dynamique des Systèmes, UMR 5513, 69134 Ecully, France*
[‡]Centre National d'Études Spatiales, 75012 Paris, France
[§]ArianeGroup SAS, 27207 Vernon Cedex, France
[¶]Safran Aircraft Engines-Villaroche, 77550 Moissy-Cramayel, France
giorgia.foschi@ec-lyon.fr · fabrice.thouverez@ec-lyon.fr · laurent.blanc@ec-lyon.fr
· giuseppe.fiore@cnes.fr · giampiero.pampolini@ariane.group · patrick.girard@safrangroup.com
[†]Corresponding author

Abstract

The need for high turbopumps efficiency makes labyrinth seals a wide diffused subsystem in space engines. The role of this non-contacting shaft seal is to reduce flow leakage and to limit recirculation through rotor/stator gaps in pumps and turbines. The high fluctuations of pressure and velocity deriving from their operation, together with the necessity for light structures, lead labyrinth seals to be subject to aeroelastic instabilities, object of in-depth investigations in order to prevent failures caused by fatigue and provide safer turbopumps. This work presents the stability analysis of a straight-through two-fins labyrinth gas seal resulting from the variation of working conditions and parameters, in order to investigate how the latters can affect the system behavior in the case of an isentropic flow and strong fluid-structure coupling.

Nomenclature

Greek Letters

γ	Specific heats ratio
ν	Kinematic viscosity [m^2 s^{-1}]
Ω	Shaft rotating velocity [rad s^{-1}]
ρ	Density [kg m^{-3}]
θ	Azimuthal position
ε	Perturbation parameter

Roman Letters

$\bar{V}$	Cavity control volume [m^3]
$\dot{m}$	Axial mass flow rate per circumferential length [kg m^{-1} s^{-1}]
A	Seal cavity transverse area [m^2]
a	Sound velocity [m s^{-1}]
B	Axial flow passage area [m^2]
C_p	Specific heat capacity [J mol^{-1} K^{-1}]
c_{in}	Fin initial clearance [m]
D_h	Hydraulic diameter
H	Total enthalpy [J]
h	Fin radial displacement [m]
h_t	Fin height [m]
L	Cavity length [m]
N	Number of teeth
n	Number of circumferential harmonics
P	Pressure [Pa]
Q	Axial mass flow rate [kg s^{-1}]
R_e	Reynolds number
R_g	Gas constant [J kg^{-1} K^{-1}]
R_s	Shaft radius [m]
T	Temperature [K]
t	Time [s]
U	Azimuthal velocity [m s^{-1}]
u	Radial displacement [m]

DOI: 10.13009/EUCASS2023-650

v	Azimuthal displacement [m]
w	Axial displacement [m]
z	Axial position
V	Axial velocity [m s^{-1}]

Subscripts

0	Steady-state solution
1	Periodic solution
i	i-th cavity
in	Inlet
out	Outlet
r	Rotor
s	Stator
tot	Total value

Superscripts

c	Associated to cosine function
s	Associated to sine function

1. Introduction

Labyrinth seals represent a fundamental system to limit turbomachinery efficiency losses: thanks to a series of teeth and cavities, they reduce the amount of fluid passing through rotor/stator gaps, therefore not contibuting to turbopump performance. The labyrinth seals particular geometry and the very small size of the gap between rotor and stator result in dangerous pressure and velocity fluctuations. The latters, together with the reduced structure thickness dictated by the need for low weight, can cause severe aeroelastic instabilities leading to dangerous structure vibrations and, in extreme cases, to turbopumps failures.
For this reason, labyrinth seals aeroelastic instabilities have been the subject of several studies since the 1960s. Alford[2] was the first to propose a stability criterion based on geometric parameters, the ratio between rotating and flexural vibration wave propagation velocities and the position of labyrinth seals support (in HP or LP zone). The latter's effective relevance in preventing failures caused by self-excited aeroelastic vibrations was then further investigated by Ehrich[11] and Abbott.[1] In particular, Ehrich drafted a stability parameter associated to the seal elastic motion caused by a pressure perturbation in the cavity. This parameter accounts for clearance dimension, system geometry and torsion centre position. Abbott, however, elaborated an analytical one-dimensional model describing labyrinth seals behaviour for given mechanical vibrations amplitude, number of nodal diameters and frequency, obtaining that stability depends to both the support position and the ratio between acoustic and mechanical frequency. Iwatsubo[15,16] studied the effect of the force induced by labyrinth seals on rotor stability through the computation of the rotordynamic stiffness and damping coefficients, assuming an isothermal flow and isentropic perturbations. Following Iwatsubo method, other authors proposed alternative versions of the 1D analytical seals model by removing some simplifying assumptions and by including new elements and hypotheses in order to obtain a more realistic representation of the system behaviour.[6,7,12] Later, Cangioli[4,5] estimated the rotordynamic coefficients by including the energy equation in the steady-state, accounting for the thermodynamic aspect of the problem. Corral and Vega[8,9,18] elaborated another stability criterion comparing the non-dimensional acoustic frequency to non-dimensional cavity discharge time.
In this paper, a stability analysis of a straight-through two-fins labyrinth gas seal is proposed assuming flexible stator, strong fluid-structure coupling and isentropic flow perturbations. The aim is to explore how the variation of some geometrical parameters and flow hypotheses can affect the nature of the interaction between the gas flowing through the seal and the stator surface and the whole system stability.

2. Fluid modelling description

In this section, an analytical one-dimensional model is developed on the basis of Childs and Scharrer[6] to describe the behaviour of the airflow passing through the labyrinth seal.

2.1 Geometry definition and hypotheses

The assumed geometry for this model is a teeth-on-rotor, one-cavity (two fins), straight-through labyrinth seal and the fluid flowing through the cavity is air, treated as a perfect gas. Pressure, temperature and azimuthal velocity are the thermodynamic parameters of the system and they are uniform in the control volume (Figures 1a and 1b). Flow velocity in the axial direction does not appear in this formulation, since the small cavity length makes it negligible with respect to the circumferential component for both the hypotheses of rotating and non-rotating shaft. Flow axial component behaviour is described by the leakage equation, linking cavity pressure P_i to inlet and outlet ones (section 2.3.1). At the exit of the labyrinth seal, the chocking condition for the axial flow is investigated and discussed. The

DOI: 10.13009/EUCASS2023-650

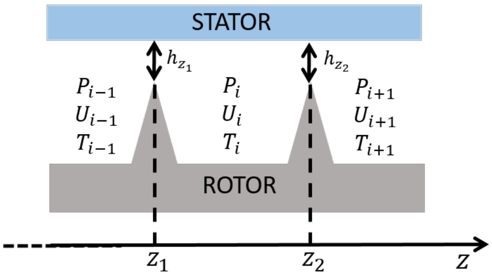

(a) Cavity 2D CV (for fixed θ)

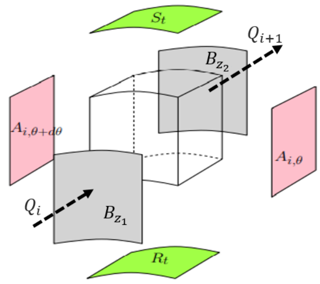

(b) Cavity 3D CV[13]

Figure 1

problem kinematic parameter is the radial clearance in correspondence of inlet and outlet tooth of the seal, respectively indicated with $h(z_1)$ and $h(z_2)$. As it will be seen in section 5, the definition of these two parameters is fundamental for the formulation of the fluid-structure coupled system. The adiabatic hypothesis is assumed for rotor and stator walls.

2.2 Governing equations

Fluid behaviour is described by Navier-Stokes equations, which integral formulation over the i-th cavity volume is normalised with respect to the azimuthal length $R_s d\theta$ and appears as follows:

- continuity equation:

$$\frac{\partial}{\partial t}(\rho_i A_i) + \frac{1}{R_s}\frac{\partial}{\partial \theta}(\rho_i U_i A_i) = \dot{m}_i - \dot{m}_{i+1} \tag{1}$$

  where $\dot{m}_i$ and $\dot{m}_{i+1}$ are respectively the cavity inlet and outlet axial mass flow for unit length (Annex A).

- circumferential momentum:

$$\frac{\partial}{\partial t}(\rho_i U_i A_i) + \frac{1}{R_s}\frac{\partial}{\partial \theta}\left(\rho_i U_i^2 A_i\right) = \dot{m}_i U_{i-1} - \dot{m}_{i+1} U_i - \frac{A_i}{R_s}\frac{\partial P_i}{\partial \theta} + \tau_{r,i} a_{r,i} L_i - \tau_{s,i} a_{s,i} L_i \tag{2}$$

  where $\tau_{r,i}$ and $\tau_{s,i}$ are respectively the fluid shear stress on rotor and stator walls and $a_{r,i}, a_{s,i}$ are non-dimensional coefficients accounting for the position of teeth (Annex B).

- energy equation

$$\frac{\partial}{\partial t}\left[\rho_i A_i \left(C_p T_i + \frac{U_i^2}{2}\right)\right] + \frac{1}{R_s}\frac{\partial}{\partial \theta}\left[\rho_i U_i A_i \left(C_p T_i + \frac{U_i^2}{2}\right)\right] = \dot{m}_i \left(C_p T_{i-1} + \frac{U_{i-1}^2}{2}\right) - \dot{m}_{i+1}\left(C_p T_i + \frac{U_i^2}{2}\right) + \frac{\partial}{\partial t}(P_i A_i) + \tau_{r,i} a_{r,i} L_i R_s \omega \tag{3}$$

System composed by Equations (1), (2) and (3) is closed by the leakage flow equation, that couples the change of pressure in the cavity with the upstream and downstream ones:

$$\dot{m}_i = f(P_{i-1}, P_i, T_i, h_{z_1}) \tag{4}$$

$$\dot{m}_{i+1} = f(P_i, P_{i+1}, T_{i+1}, h_{z_2}) \tag{5}$$

Different models for axial mass flow are assumed for the present analysis, as described in 2.3.1.

2.3 Stability parameters analysis

In this work, the response of a single-cavity labyrinth gas seal to the variation of some parameters is investigated and analysed in order to analyse which of these quantities mostly influence the subsystem behaviour . In particular, the stability of the system is studied assuming different leakage flow models and multiple values for inlet pressure and initial radial gap. At the end of the analysis, configurations with stator support location in HP zone and three cavities are also tested.

DOI: 10.13009/EUCASS2023-650

2.3.1 Leakage flow model

The leakage flow behaviour strictly depends on the variation of pressure through the labyrinth seal. Among the various existing models, the ones assumed in this article are the following:

- Neumann equation[6]

$$\dot{m}_i = \mu_0 C_d \bar{B}_{z_1} \sqrt{\frac{P_{i-1}^2 - P_i^2}{R_g T_i}} \tag{6}$$

  It is a classical empirical leakage flow equation, widely used to treat problems of compressible flows through a seal. It contains the following semi-empirical coefficients:

  - carry-over coefficient, function of geometry and number of teeth:

  $$\mu_0 = \sqrt{\frac{N}{(1-\beta_i)\, N + \beta_i}}$$

  where $\beta_i = 1 - \left(1 + 16.6 \frac{h_{z_1}}{L_i}\right)^{-2}$

  - discharge coefficient, function of pressure distribution along the seal and derived from Chaplygin formulation:[14]

  $$C_d = \frac{\pi}{\pi + 2 - 5 s_i + 2 s_i^2}$$

  where $s_i = -1 + \left(\frac{P_{i-1}}{P_i}\right)^{\frac{\gamma-1}{\gamma}}$

  As described by Szymanski,[17] many authors took Neumann leakage flow model and redefined carry-over and discharge coefficients, elaborating new versions of equation (6):

- Scharrer kept Neumann's discharge coefficient, but rewrote the carry-over one as follows:

$$\mu_0 = \sqrt{\frac{1}{1-\alpha_i}}$$

  where $\alpha_i = \dfrac{8.52}{\frac{t_i - b_i}{h_{z_1}} + 7.23}$ and t_i, b_i are indicated in Figure 2.

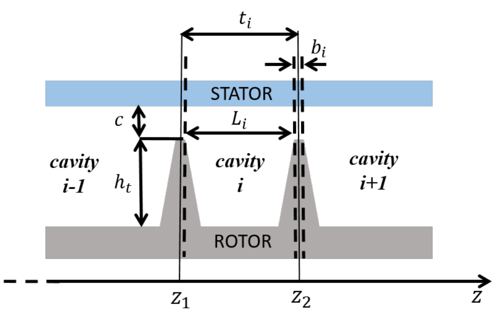

Figure 2: Cavity geometrical parameters definition

- Esser and Kazakia derive from CFD a constant discharge coefficient:

$$C_d = 0.716$$

- Kurohashi rewrote the carry-over coefficient as a function of the jet expansion angle of the seal (optically measured as 6°):

$$\mu_i = \begin{cases} \sqrt{\dfrac{1}{1-\alpha_i+\alpha_i^2}}, & \text{for } i = 1 \\ \sqrt{\dfrac{1}{1-2\alpha_i+\alpha_i^2}}, & \text{for } i > 1 \end{cases}$$

DOI: 10.13009/EUCASS2023-650

where $\alpha_i = \frac{\frac{h_i}{t_i - b_i}}{\frac{h_i}{t_i - b_i} C_d + \tan 6^\circ}$.

Other two leakage flow models are included in this analysis:

- the expression of an incompressible laminar flow through an orifice:

$$\dot{m}_i = C_d \bar{B}_{z_1} \sqrt{2\rho_i (P_{i-1} - P_i)}, C_d = 0.61 \tag{7}$$

- the isentropic mass-flow equation:

$$\dot{m}_i = \frac{P_{tot,i-1} \bar{B}_{z_1}}{\sqrt{R_g T_{tot,i}}} \left(\frac{P_{tot,i-1}}{P_i} \right)^{-\frac{\gamma+1}{2\gamma}} \sqrt{\frac{2\gamma}{\gamma - 1} \left[\left(\frac{P_{tot,i-1}}{P_i}^{\frac{\gamma-1}{\gamma}} \right) - 1 \right]} \tag{8}$$

3. Linearized problem

The linearisation process represents an effective way to simplify the resolution of a non-linear differential equations system. In this work the linearised problem is obtained by using a small perturbation method, through which each parameter is expressed by a power series expansion truncated at the first order:

$$\begin{aligned}
h_i (t, \theta) &= h_{0,i} + \varepsilon h_{1,i} (t, \theta) \\
P_i (t, \theta) &= P_{0,i} + \varepsilon P_{1,i} (t, \theta) \\
U_i (t, \theta) &= U_{0,i} + \varepsilon U_{1,i} (t, \theta) \\
T_i (t, \theta) &= T_{0,i} + \varepsilon T_{1,i} (t, \theta) \\
A_i (t, \theta) &= A_{0,i} + \varepsilon A_{1,i} (t, \theta) \\
\dot{m}_i (t, \theta) &= \dot{m}_{0,i} + \varepsilon \dot{m}_{1,i} (t, \theta)
\end{aligned} \tag{9}$$

For each of them, the constant term represents the problem steady-state solution and the first-order one represents the perturbed state solution.
Fluctuations of axial mass-flow rate and cavity transverse area are functions of the oscillations of the other thermodynamic parameters:

- Transverse area $A_{1,i}$ strictly depends on the tip clearance $h_{1,i}$, linked to the radial shift of the stator surface (section 4):

$$A_{1,i} (t, \theta) = \int_0^L h_{1,i}(z) dz \tag{10}$$

- Axial mass-flow rates $\dot{m}_{1,i}$ and $\dot{m}_{1,i+1}$ depend on first-order radial gap, pressure and temperature:

$$\dot{m}_{1,i} (t, \theta) = A^{\dot{m}}_{0,i} h_{1,z_1} + B^{\dot{m}}_{0,i} P_{1,i-1} + C^{\dot{m}}_{0,i} P_{1,i} + D^{\dot{m}}_{0,i} T_{1,i} \tag{11}$$

$$\dot{m}_{1,i+1} (t, \theta) = A^{\dot{m}}_{0,i+1} h_{1,z_2} + B^{\dot{m}}_{0,i+1} P_{1,i} + C^{\dot{m}}_{0,i+1} P_{1,i+1} + D^{\dot{m}}_{0,i+1} T_{1,i+1} \tag{12}$$

The expression of coefficients $A^{\dot{m}}, B^{\dot{m}}, C^{\dot{m}}, D^{\dot{m}}$ depends on the adopted model for $\dot{m}$ (section 2.3.1).

After replacing (9) in the conservation equations system, this one is reformulated in two ways:

- zero-order system, which solution gives the steady-state
- first-order system, which solution gives the perturbation state

3.1 Zero-order system

For a stationary flow, equations of section 2.2 assume the following form:

$$\begin{cases}
\dot{m}_{0,i+1} = \dot{m}_{0,i} = \dot{m}_0 \\
\dot{m}_0 (U_{0,i} - U_{0,i-1}) = \tau_{r_{0,i}} a_{r_{0,i}} L_i - \tau_{s_{0,i}} a_{s_{0,i}} L_i \\
\dot{m}_0 \left(C_p T_{0,i} + \frac{U_{0,i}^2}{2} \right) - \dot{m}_0 \left(C_p T_{0,i-1} + \frac{U_{0,i-1}^2}{2} \right) = \tau_{r_{0,i}} a_{r_{0,i}} L_i R_s \Omega
\end{cases} \tag{13}$$

DOI: 10.13009/EUCASS2023-650

The adopted model for shear stress on rotor and stator walls is Blasius equation for turbulent flow through smooth pipes:[10]

$$\begin{aligned} \tau_{ri} &= \frac{1}{2}\rho_i C_{fr_i} (R_s\Omega - U_i)^2 \\ \tau_{si} &= \frac{1}{2}\rho_i C_{fs_i} U_i^2 \end{aligned} \tag{14}$$

Friction coefficients C_{fr_i} and C_{fs_i} have been defined through a mixed model, that would be called "Colebrook model" and that assumes different laws for the friction coefficient, depending on the value of Re number:

- for $R_e \leq 1000$: Blasius law for a laminar flow in smooth pipes:

$$C_f = \frac{24}{R_e} \tag{15}$$

- for $R_e \geq 3000$: Colebrook implicit law for a turbulent flow in rough pipes:

$$\begin{aligned} x &= a - b\log\left(\frac{g}{D_h} + \frac{c}{R_e}x\right) \\ C_{fk} &= \frac{1}{4x^2} \end{aligned} \tag{16}$$

where g is the roughness and a and b two empirical coefficients.

- for $1000 \leq R_e \leq 3000$: Zirkelback and San Andres[19] law:

$$\begin{aligned} \xi &= \frac{R_e - 1000}{3000 - 1000} \\ C_f &= C_{fb}(R_e)\left[1 + \xi^2(2\xi - 3)\right] + C_{fk}(R_e, g)\xi^2(3 - 2\xi) \end{aligned} \tag{17}$$

Assuming an isentropic stationary flow, for which $\tau_{0,i} = 0$, system (13) becomes:

$$\begin{cases} \dot{m}_{0,i+1} = \dot{m}_{0,i} = \dot{m}_0 \\ U_{0,i} = U_{0,i-1} = U_0 \\ T_{0,i} = T_{0,i-1} = T_0 \end{cases} \tag{18}$$

However, system (18) is not representative of flow behaviour in the case of $U_{in} = 0$ m/s, because flow velocity is not affected by the presence of stator and rotor walls and by the shaft rotating velocity, so flow tangential velocity would be null all along the seal.

3.1.1 Chocked flow hypothesis

Given the inlet pressure, temperature and velocity and the outlet pressure as input parameters, the solution of the stationary problem is possible by imposing the chocked flow condition at the last seal tooth. This assumption allows to dispose of a first evaluation of the axial mass flow rate, necessary to make an estimation of pressure in the cavity. For a chocked compressible flow, in fact, $P_{out}/P_i = 0.528$ and the mass-flow rate outgoing the cavity is defined by Fliegner as follows:

$$\dot{m}_{0,i+1} = \frac{0.510\mu_0}{\sqrt{R_g T_i}} P_i \bar{B}_{z_2} \tag{19}$$

Equation (19), together with an expression for the leakage flow (2.3.1), closes the system of equations (1), (2) and (3).
Therefore, it is possible to compute the value of pressure in the cavity P_i and at inlet of the seal $P^{'}_{in}$. By comparing this one with the input parameter P_{in} it is possible to verify if the chocking condition occurs or not:

- if $P^{'}_{in} < P_{in}$, chocking condition is verified: P_i is adjusted and the inlet pressure is re-calculated up to get $P^{'}_{in} - P_{in} \simeq 0$, so the control parameter is the input inlet pressure P_{in}
- if $P^{'}_{in} > P_{in}$, chocking condition is not verified: P_{in} is adjusted and the outlet pressure is re-calculated up to get $P^{'}_{out} - P_{out} \simeq 0$, so the control parameter is P_{out}.

DOI: 10.13009/EUCASS2023-650

3.2 First-order system

The perturbed state system of equations is obtained by applying the small perturbation method to (1),(2) and (3), leading to the system rotor dynamic coefficients and linearised conservation equations (Appendix C).
The solution in terms of pressure, azimuthal velocity, temperature and radial displacement is assumed to be a periodic function of the type:

$$y_{1,i}(t,\theta) = \sum_{n=1}^{K} y_n^c \cos(n\theta) + y_n^s \sin(n\theta) \tag{20}$$

where n is the number of the harmonic.
In order to simplify the system solution and to decouple the contribution of each harmonic from the other ones, (20) is substituted in the first-order equations and a Galerkin approach is used, leading to a linear algebraic problem:

$$\tilde{A}_i \dot{Y}_{1,i,n}(t) + \tilde{B}_i Y_{1,i,n}(t) = 0. \tag{21}$$

where $Y_{1,i,n} = \left[h_{z_1}^c, h_{z_1}^s, P_i^c, P_i^s, U_i^c, U_i^s, T_i^c, T_i^s\right]_{1,n}^T$ are the variables of the problem and matrices $\tilde{A}_i$ and $\tilde{B}_i$ have the following structure:

$$\begin{aligned}\tilde{A}_i &= [\tilde{A}_{fs}, \tilde{A}_{ff}]_i \\ \tilde{B}_i &= [\tilde{B}_{fs}, \tilde{B}_{ff}]_i\end{aligned} \tag{22}$$

The sub-matrices $[\tilde{A}_{fs}]_i$ and $[\tilde{B}_{fs}]_i$ contain the fluid-structure coupling coefficients, while $[\tilde{A}_{ff}]_i$ and $[\tilde{B}_{ff}]_i$ components are only referred to the fluid.

4. Structure modelling

The structural part of the studied system is composed by a rigid rotating shaft and a flexible stator. Its dynamic behaviour is described by the following system:

$$[M]\ddot{X} + [K]X = F(t) \tag{23}$$

X is the structural displacement and can be expressed as:

$$X = \sum_{n=1}^{K} q_n(t)\psi_n = \Psi\bar{q} \tag{24}$$

where ψ_n is the vector of modal shapes for each n mode and q_n is the generalised displacement vector.
If we consider mass-normalised structural modes:

$$\Psi^T [M]\Psi = 1 \tag{25}$$

and we substitute (24) in (23), by exploiting the properties of normal modes system (23) can be rewritten as n uncoupled equations of the type:

$$\ddot{\bar{q}}_n + \left[\tilde{K}\right]\bar{q}_n = \frac{\partial W}{\partial q_n} \tag{26}$$

If we consider only the dual modes, $\left[\tilde{K}\right]$ results in a block diagonal matrix with the same value of the eigenfrequency ω_j in each 2x2 block:

$$\left[\tilde{K}\right] = \begin{bmatrix} \begin{bmatrix}\omega_1^2 & 0 \\ 0 & \omega_1^2\end{bmatrix} & \cdots & 0 \\ \vdots & \ddots & \vdots \\ 0 & \cdots & \begin{bmatrix}\omega_{n/2}^2 & 0 \\ 0 & \omega_{n/2}^2\end{bmatrix} \end{bmatrix}$$

Eigenfrequencies are obtained from a classical FE code.[3] To solve equation (26) it's necessary to calculate the work W carried out by the fluid on the stator internal surface.

DOI: 10.13009/EUCASS2023-650

4.1 Fluid work computation

Within the seal, the work of fluid on stator is defined as:

$$W = \int_0^L \int_0^{2\pi} P(\theta, z, t)\, \vec{n}\vec{u} R_{st}\, d\theta dz \tag{27}$$

where $P(\theta, t)$, $\vec{n}$ and $\vec{u}$ are, respectively, the pressure exerted by the fluid, the surface normal vector and the stator surface displacement. As already seen for the fluid modelling parameters, also $\vec{n}$ and $\vec{u}$ can be expressed in the form (9):

$$\begin{aligned} P_i(t,\theta) &= P_{0,i} + \varepsilon P_{1,i}(t,\theta) \\ \vec{n}(t,z,\theta) &= \vec{n}_0(z) + \varepsilon \vec{n}_1(t,z,\theta) \\ \vec{u}(t,z,\theta) &= \vec{u}_0(z) + \varepsilon \vec{u}_1(t,z,\theta) \end{aligned} \tag{28}$$

4.1.1 Displacement vector

The value of the zero-order structure displacement vector is obtained through a finite elements analysis with Ansys Mechanical APDL. Knowing the value of vector $\vec{u}_{0,i}$ components at the nodes, a least squares interpolation of these values has been done with a 20th degree polynomials in order to obtain the expression of $u_{0,i}$, $v_{0,i}$ and $w_{0,i}$ as functions of the axial direction z:

$$\begin{aligned} u_0(z) &= a_{20}z^{20} + ... + a_1 z + a_0 \\ v_0(z) &= b_{20}z^{20} + ... + b_1 z + b_0 \\ w_0(z) &= c_{20}z^{20} + ... + c_1 z + c_0 \end{aligned} \tag{29}$$

The process to obtain the first-order displacement vector is similar to the previous one: once the values of cosinus and sinus components of $\vec{u}_{1,i}$ have been calculated through a modal analysis of the stator, an interpolation with polynomials of degree 12 has been done to obtain $u^{c,s}_{1,i,n}$,$v^{c,s}_{1,i,n}$ and $w^{c,s}_{1,i,n}$ on the axial direction z:

$$\begin{aligned} u^{c,s}_{1,n}(z) &= a^{c,s}_{12,n}z^{12} + ... + a^{c,s}_{1,n}z + a^{c,s}_{0,n} \\ v^{c,s}_{1,n}(z) &= b^{c,s}_{12,n}z^{12} + ... + b^{c,s}_{1,n}z + b^{c,s}_{0,n} \\ w^{c,s}_{1,n}(z) &= c^{c,s}_{12,n}z^{12} + ... + c^{c,s}_{1,n}z + c^{c,s}_{0,n} \end{aligned} \tag{30}$$

Finally, the first-order displacement vector is:

$$\begin{aligned} \vec{u}_1(t,z,\theta) = &\left[\sum_n q_{1,n}(t)^c u^c_{1,n}(z)\cos(n\theta) + q_{1,n}(t)^s u^s_{1,n}(z)\sin(n\theta)\right]\vec{e}_r \\ &+ \left[\sum_n q_{1,n}(t)^c v^c_{1,n}(z)\cos(n\theta) + q_{1,n}(t)^s v^s_{1,n}(z)\sin(n\theta)\right]\vec{e}_\theta \\ &+ \left[\sum_n q_{1,n}(t)^c w^c_{1,n}(z)\cos(n\theta) + q_{1,n}(t)^s w^s_{1,n}(z)\sin(n\theta)\right]\vec{e}_z \end{aligned} \tag{31}$$

where $q^c_{1,n}$, $q^s_{1,n}$ are the unknowns parameters to be determined.

4.1.2 Normal vector

Once the displacement vector has been defined, stator internal surface normal vector can be determined by the following equation:

$$\vec{n}_1 = \frac{\vec{N}_1}{||\vec{N}_1||} \text{ with } \vec{N}_1(t,z,\theta) = \frac{\partial \vec{u}_1(t,z,\theta)}{\partial z} \times \frac{\partial \vec{u}_1(t,z,\theta)}{\partial \theta} \tag{32}$$

The expression of the work done by fluid on the structure can now be computed through (27) in order to obtain the expression for $\frac{\partial W}{\partial q_j}$ in the dynamic equation (26). The result is a new final expression of the dynamic system:

$$\ddot{\bar{q}}_{1,n} + \left[\tilde{K}\right]_{1,n} \bar{q}_{1,n} - [F]_{1,i} P_{1,i,n} = 0 \tag{33}$$

DOI: 10.13009/EUCASS2023-650

If we put the generalised displacement operators and the pressure in the same variables vector, obtaining: $\bar{X}_{1,n} = [q^c, q^s, P_i^c, P_i^s, U_i^c, U_i^s, T_i^c, T_i^s]_{1,n}^T$, equation (33) becomes:

$$\ddot{\bar{X}}_{1,n} + \left[\bar{K}\right] \bar{X}_{1,n} = 0 \tag{34}$$

where $\left[\bar{K}\right] = [\bar{K}_{ss}, \bar{K}_{sf}]$. Sub-matrices $[\bar{K}_{ss}]$ and $[\bar{K}_{sf}]$ contain the stiffness coefficients of, respectively, the mechanical and fluid-structure coupled system.

5. Fluid-structure coupling system

In order to study the stability of the labyrinth seal, it is necessary to solve the system derived from the coupling between the fluid and the mechanical model. To this end, a strong fluid-structure coupling has been considered, that allows to write the following relation for the radial structure displacement in correspondence of the two teeth of the cavity:

$$\begin{aligned} h_{1,z_1,n}(t,\theta) &= u_{1,z_1,n}(t,\theta) \\ h_{1,z_2,n}(t,\theta) &= u_{1,z_2,n}(t,\theta) \end{aligned} \tag{35}$$

Through (31), radial clearance in correspondence of the two teeth assumes the following form:

$$\begin{aligned} h_{1,z_1,n} &= \sum_{i,n} q_n(t)^c u_{1,z_1,n}^c \cos(n\theta) + q_n(t)^s u_{1,z_1,n}^s \sin(n\theta) \\ h_{1,z_2,n} &= \sum_{i,n} q_n(t)^c u_{1,z_2,n}^c \cos(n\theta) + q_n(t)^s u_{1,z_2,n}^s \sin(n\theta) \end{aligned} \tag{36}$$

Therefore, sinus and cosinus components h_{1,z_1} and h_{1,z_2} can be expressed as function of the generalised displacement variables q_n^c and q_n^s, representing the only kinematic variables of the problem:

$$\begin{aligned} h_{1,z_1,n}^{c,s} &= q_n(t)^{c,s} u_{1,z_1,n}^{c,s} \\ h_{1,z_2,n}^{c,s} &= q_n(t)^{c,s} u_{1,z_2,n}^{c,s} \end{aligned} \tag{37}$$

The resulting global system is of the form:

$$[\tilde{A}_c]\ddot{\bar{X}}_{1,n} + [\tilde{B}_c]\dot{\bar{X}}_{1,n} + [\tilde{C}_c]_i \bar{X}_{1,n} = 0. \tag{38}$$

where the coupled system matrices $[\tilde{A}_c]$, $[\tilde{B}_c]$ and $[\tilde{C}_c]$ have dimension 8×8 and have structure:

$$[\tilde{A}_c] = \begin{bmatrix} \begin{bmatrix} 1 & 0 \\ 0 & 1 \end{bmatrix} & \begin{bmatrix} 0 & \cdots & 0 \\ 0 & \cdots & 0 \end{bmatrix} \\ \begin{bmatrix} 0 & 0 \\ \vdots & \vdots \\ 0 & 0 \end{bmatrix} & \begin{bmatrix} 0 & \cdots & 0 \\ \vdots & \ddots & \vdots \\ 0 & \cdots & 0 \end{bmatrix} \end{bmatrix}, [\tilde{B}_c] = \begin{bmatrix} \begin{bmatrix} 0 & 0 \\ 0 & 0 \end{bmatrix} & \begin{bmatrix} 0 & \cdots & 0 \\ 0 & \cdots & 0 \end{bmatrix} \\ [\tilde{A}_{fs}] & [\tilde{A}_{ff}] \end{bmatrix}, [\tilde{C}_c] = \begin{bmatrix} [\bar{K}_{ss}] & [\bar{K}_{sf}] \\ [\tilde{B}_{fs}] & [\tilde{B}_{ff}] \end{bmatrix} \tag{39}$$

The coupled system stability parameter (damping ratio) and frequency are computed as follows:

$$\zeta_k = -\frac{Re(\lambda_k)}{|\lambda_k|}, f_k = \frac{1}{2\pi} \frac{Im(\lambda_k)}{\sqrt{1 - \zeta_k}} \tag{40}$$

where the complex eigenvalues λ_n are obtained from the solution of system (38). By convention, a negative value of the damping ratio ζ_k is associated to an unstable system.

6. Results

In this section, an analysis of the previously described system stability to different operating conditions and parameters is presented. Geometrical characteristics and input data for the assumed configurations are summarised in Table 1. To each one corresponds a specific hypothesis for:

- the number of cavities N
- the inlet pressure P_{in}
- the initial value of the radial clearance c_{in}

DOI: 10.13009/EUCASS2023-650

Configuration	C_0	C_1	C_2	C_3	C_4	C_5	C_6
Number of cavities	1	1	1	1	1	1	3
Inlet pressure P_{in} [bar]	3	3	3	7	3	3	3
Initial radial clearance $c_{in}[\mu m]$	150	150	150	150	300	150	150
Leakage model	Neumann	Isentropic	Incompressible	Neumann	Neumann	Neumann	Neumann
Stator support location	LP	LP	LP	LP	LP	HP	LP

Table 1: Studied configurations. Input invariant parameters: T_{in} = 293 K, U_{in} = 0 m/s , P_{out} = 1.01 bar, R_s = 0.0764 m, L_s = 0.15 m, n = 2

Leakage model	Neumann	Scharrer	Esser & Kazakia	Kurohashi	Isentropic	Incompressible
$\dot{m}_0$[kg/s]	0.0325	0.0321	0.0335	0.0323	0.0364	0.0302
P_{C0} [bar]	2.34	2.34	2.42	2.34	2.63	2.18

Table 2: Zero-order values of pressure and axial mass-flow rate for different leakage-flow expressions

- the adopted model for the axial leakage flow
- the location of the stator support, that can be in low pressure side (LP) or high pressure side (HP)

As showed in Table 2, the leakage flow models of Neumann, Scharrer, Esser & Kazakia and Kurohashi give very similar values of axial mass-flow rate and cavity pressure for the steady-state system, while the isentropic and the incompressible leakage flow laws respectively give a higher and lower value of $\dot{m}_0$. For this reason, only Neumann, isentropic and incompressible axial mass-flow models are assumed in the present analysis.
The first-order solution of the fully-coupled system in terms of frequency and damping is evaluated for a range of increasing shaft rotating velocity values, considering a solicitation mode of 2 nodal diameters.
Figure 3 shows the coupled system frequencies and stability behaviour for increasing values of the shaft rotation velocity for configuration C_0. In particular, dashed lines in Figure 3a represent the uncoupled frequencies, which for n = 2 are:

- for the acoustic case: $f_{ac} = \dfrac{na}{2\pi R_s} \pm \dfrac{nU}{2\pi R_s}$
- for the structure: f_{st} = 1713.6 Hz

The uncoupled acoustic frequencies appear higher than the coupled system ones: this is the effect of a strong fluid-structure coupling, that reduces the value of the frequencies associated with the fluid. On the contrary, by observing the mechanical system frequencies, the uncoupled ones are lower than the ones derived from the coupling. This is the effect of a stiffness increase, which occurs when the mechanical frequency is high. Moreover, the coupling between structure and Ω appears much weaker with respect to the fluid: the two modes in which the structural one is split into for an increasing Ω are very close. In the present case, structure frequencies are significantly higher than acoustic ones: in this condition, as showed in Figure 3b, the damping ratio associated with the structure remains positive with Ω , giving a stable system. This result agrees with Abbott[1] criterion, by which the system is stable if the stator support is located in the LP zone and $f_{st} > f_{ac}$.

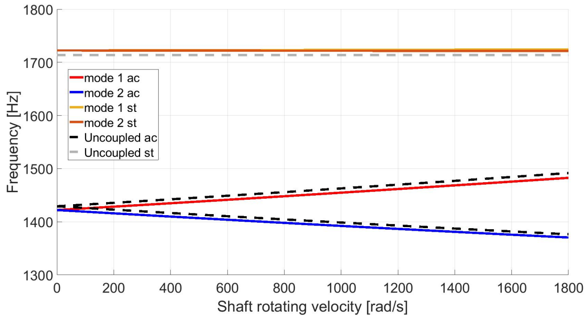

(a) C_0 configuration: frequencies

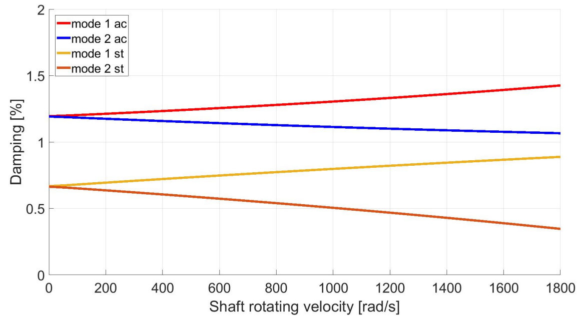

(b) C_0 configuration: damping ratios

Figure 3: C_0 configuration: frequencies and damping ratios for Neumann leakage-flow model.

DOI: 10.13009/EUCASS2023-650

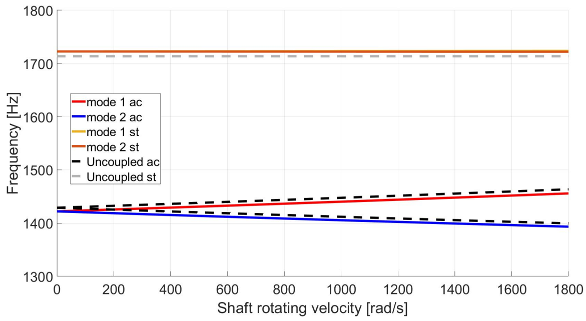

(a) C_1 configuration: frequencies

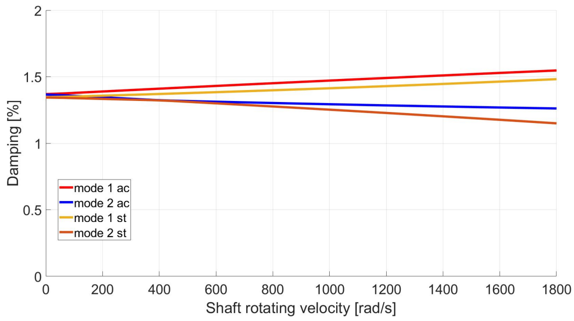

(b) C_1 configuration: damping ratios

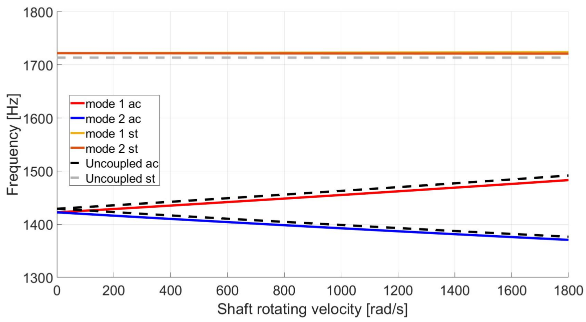

(c) C_2 configuration: frequencies

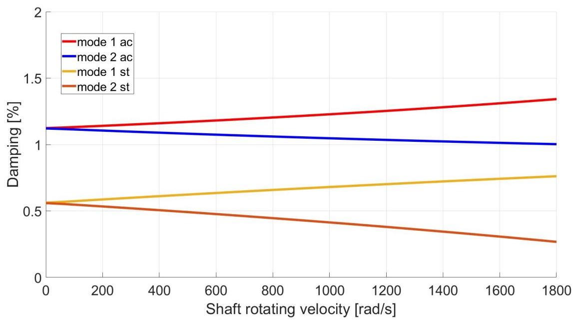

(d) C_2 configuration: damping ratios

Figure 4: C_1 and C_2 configurations: frequencies and damping ratios for different leakage flow models

6.1 Leakage flow model impact

The influence that leakage flow model has on fluid-structure coupled system frequency and damping ratio can be observed in Figure 4, where the results obtained with the isentropic leakage flow model (configuration C_1, Figures 4a-4b) are compared with those deriving from the incompressible leakage flow model assumption (configuration C_2, Figures 4c-4d).
For the same pressure drop, these two models respectively give a higher and lower value of $\dot{m}_0$ with respect to Neumann model of configuration C_0. The effect of such difference is a different opening of the coupled system frequencies curves. In particular, when a higher leakage mass flow is assumed (Figure 4a) the variation of the acoustic frequencies with the shaft rotation velocity is more limited, revealing a weaker coupling with Ω.
From the point of view of stability, a higher mass flow rate determines a more stable system (Figure 4b) since the damping ratio curves of configuration C_2 shift upward and decrease their opening with respect to the results previously showed for configuration C_0.

6.2 Inlet pressure impact

In order to investigate how a change in the inlet pressure value can influence the studied system stability behaviour, configuration C_3 is tested: it is identical to C_0, but is assumes an inlet pressure passing from P_{in} = 3 bar to P_{in} = 7 bar. The effect of this variation is showed in Figure 5: a higher upward pressure determines a higher difference between the uncoupled and coupled system frequencies, from both the acoustic and the mechanical point of view. When the pressure drop increases, the axial mass flow passing through the clearance increases too, leading the frequencies associated with the fluid of the coupled system to be more affected by the presence of the mechanical part. In these conditions the system becomes unstable, as showed in Figure 5b, where the structural damping ratio appears negative. This can be traced to the sub-matrix $[\tilde{B}_{fs}]$ that couples the fluid behaviour to the stator internal surface one. The increase of the coefficients of this sub-matrix leads to a destabilising effect on the coupled system.

6.3 Radial clearance impact

The influence of radial clearance can be observed by comparing the results previously analysed for $c_{in} = 150\mu m$ (Figure 3) with those referred to the configuration C_4 with $c_{in} = 300\,\mu m$ of Figure 6. The assumption of a higher space between

DOI: 10.13009/EUCASS2023-650

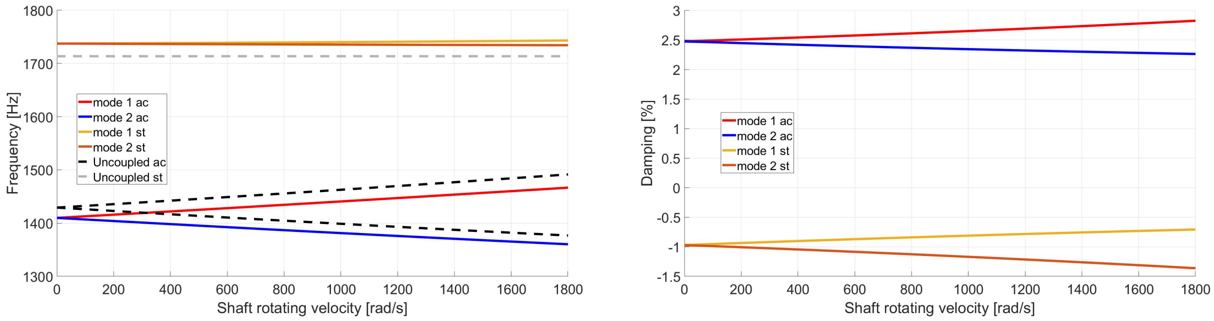

(a) C_3 configuration: frequencies

(b) C_3 configuration: damping ratios

Figure 5: C_3 configuration: frequencies and damping ratios for P_{in} = 7 bar.

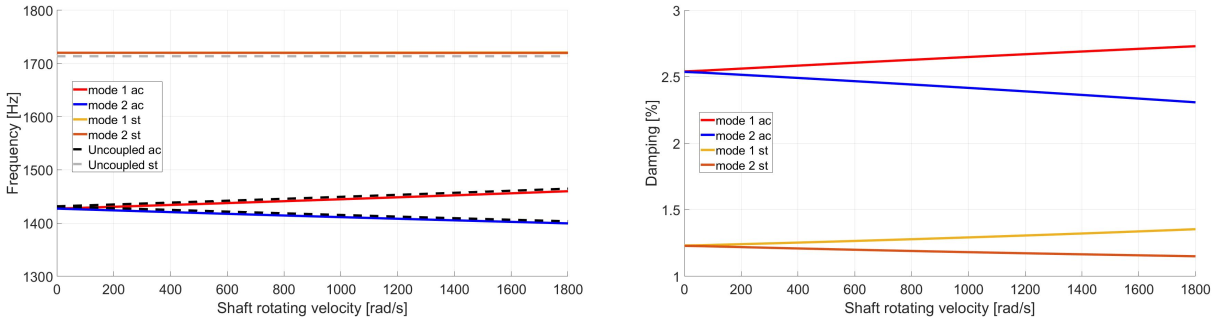

(a) C_4 configuration: frequencies

(b) C_4 configuration: damping ratios

Figure 6: C_4 configuration: frequencies and damping ratios for $c = 300\mu m$.

the top of the labyrinth seal teeth and the stator internal surface determines a lower coupling between acoustic wave and Ω as it can be seen in Figure 6a, where the difference between forward and backward acoustic modes is lower with respect to configuration C_0.
From the point of view of stability, the choice of a higher radial clearance has a stabilizing effect on the system: the mechanical damping ratio curves in Figure 6b are shifted to higher values with respect to Figure 3b, which is stable too.

6.4 Stator support position impact

The influence of the position in which stator support is located on system stability represents another interesting aspect to be investigated. By comparing the results obtained for configuration C_0 (Figure 3, LP configuration for P_{in} = 3 bar) with the ones represented in Figure 8 (HP configuration for P_{in} = 3 bar), it is evident that the seal damping ratio reverses its sign according to the zone to which stator is connected. In particular, for the specific case where $f_{st} > f_{ac}$, a support in the HP zone makes the system unstable, while it is stable in the case $f_{st} < f_{ac}$. This trend comes from the change of the sign of matrix $[\tilde{B}_{fs}]$ diagonal coefficient $G_{9,i}$ (Appendix C) deriving from the conservation equations: this coefficient depends on the difference between the value assumed by the stator internal surface static displacement in correspondence of the inlet and the outlet tooth. When the LP configuration is assumed (Figure 7a), as a result of the pressure exerced by fluid on the stator surface, the radial clearance in correspondence to axial position z_1 is higher than the one in z_2. In the HP configuration (Figure 7b) we have the opposed situation, as high pressure acts on the zone where stator is constrained. As consequence, the above mentioned coefficient of the coupling fluid-structure sub-matrix changes its sign and contributes in two opposed ways to the system stability.

6.5 Number of cavities impact

For the sake of completeness of this analysis, Figure 9 shows the results obtained by considering a labyrinth seal with inlet pressure P_{in} = 7 bar and 3 cavities. It is interesting to observe the differences between frequency and damping ratio variation with Ω for this configuration and the ones, previously analysed, obtained for the one-cavity configuration

DOI: 10.13009/EUCASS2023-650

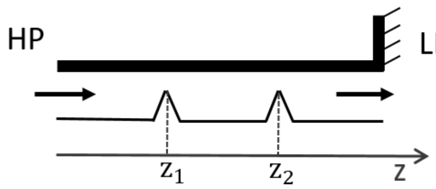

(a) LP configuration

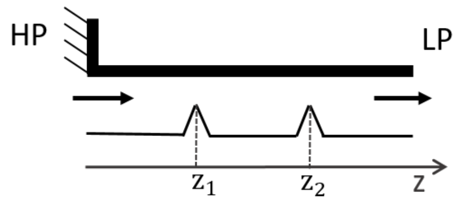

(b) HP configuration

Figure 7

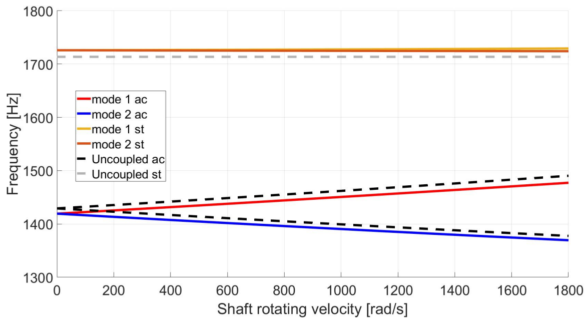

(a) C_5 configuration: frequencies

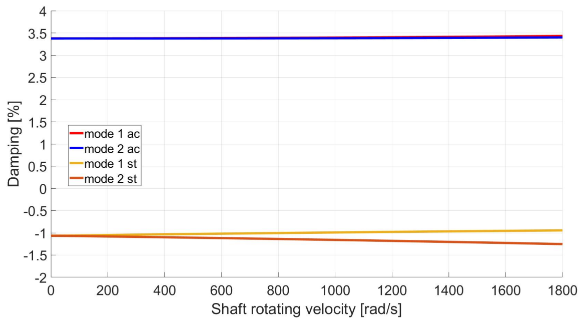

(b) C_5 configuration : damping ratios

Figure 8: C_5 configuration: frequencies and damping ratios when stator support is in HP zone.

C_3 (Figure 5). By observing the coupled frequencies of the 3 cavities seal in Figure 9a, we can notice that for each cavity there is a pair of acoustic waves and that each of them assumes a different value starting at $\Omega = 0$ rad/s. This is due to the variation that fluid pressure undergoes passing through the seal. As regards damping, by comparing the values derived from configuration C_3 for a unique cavity (Figure 5b) with those obtained for 3 cavities (Figure 9b) one identifies that a higher value of N tends to stabilise the system. In fact, while the configuration with one cavity and $P_{in} = 7$ bar in always unstable with Ω, the one with more cavities shows the birth of an aeroelastic instability (associated to the last cavity) for $\Omega \geq 900$ rad/s.

7. Conclusions and perspectives

The present work investigates the stability and fluid-structure coupling of a two-fins labyrinth gas seal as function of different parameters and working conditions. To this purpose, an accurate approach to properly study labyrinth seals aeroelastic behaviour is proposed through the development of an analytical one-dimensional fluid-structure coupled system model. This one assumes a strong interaction between gas flow and system rotordynamics, under the hypothesis of rigid rotor, flexible stator and isentropic fluid parameters fluctuations. The obtained results reveal a particular

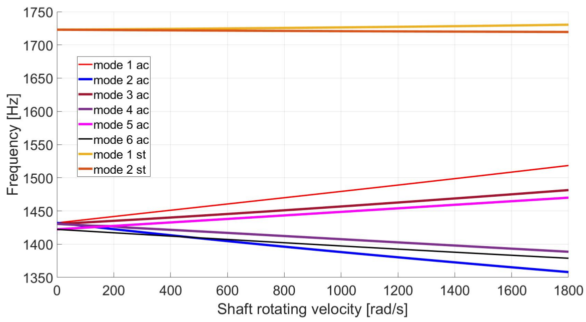

(a) C_6 configuration: frequencies

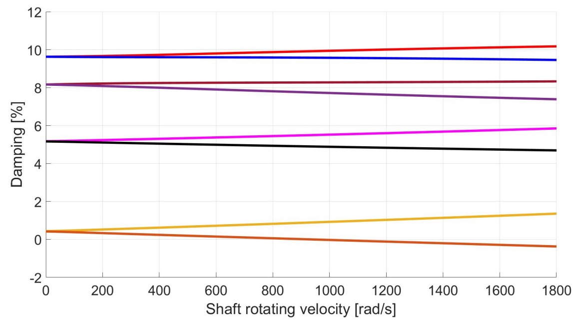

(b) C_6 configuration: damping ratios

Figure 9: C_6 configuration: frequencies and damping ratios for $N = 4$

DOI: 10.13009/EUCASS2023-650

sensitivity of global system stability to radial clearance dimension and number of cavities, as well as to the adopted model for leakage flow, the value of the inlet pressure and the position of the stator support. These achievements are consistent with literature, in particular with the results obtained by Abbott for the case of a structural frequency much higher than acoustic one. The future perspectives deriving from these achievements are the improvement of the analytical model representativeness, by including the thermodynamic aspect and dissipative effects, and the numerical results validation through an experimental campaign on an existing test bench in development phase.

8. Acknowledgments

The authors are grateful to Centre National d'Études Spatiales and ArianeGroup SAS for providing the financial support for this project.

References

[1] DR Abbott. Advances in labyrinth seal aeroelastic instability prediction and prevention. 1981.

[2] JS Alford. Protection of labyrinth seals from flexural vibration. 1964.

[3] Inc. ANSYS. Ansys mechanical apdl structural analysis guide, release 16.1, 2021.

[4] Filippo Cangioli, Paolo Pennacchi, Giuseppe Vannini, and Lorenzo Ciuchicchi. Effect of energy equation in one control-volume bulk-flow model for the prediction of labyrinth seal dynamic coefficients. *Mechanical Systems and Signal Processing*, 98:594–612, 2018.

[5] Filippo Cangioli, Paolo Pennacchi, Giuseppe Vannini, Lorenzo Ciuchicchi, Andrea Vania, Steven Chatterton, and Phuoc Vinh Dang. On the thermodynamic process in the bulk-flow model for the estimation of the dynamic coefficients of labyrinth seals. *Journal of Engineering for Gas Turbines and Power*, 140(3), 2018.

[6] Dara Childs. *Turbomachinery rotordynamics: phenomena, modeling, and analysis*. John Wiley & Sons, 1993.

[7] Dara W Childs and Joseph Kirk Scharrer. An iwatsubo-based solution for labyrinth seals: comparison to experimental results. 1986.

[8] Roque Corral, Michele Greco, and Almudena Vega. Higher order conceptual model for labyrinth seal flutter. *Journal of Turbomachinery*, 143(7), 2021.

[9] Roque Corral and Almudena Vega. Conceptual flutter analysis of labyrinth seals using analytical modelsâpart i: Theoretical support. *Journal of Turbomachinery*, 140(12):121006, 2018.

[10] Rohan J DâSouza and Dara W Childs. A comparison of rotordynamic-coefficient predictions for annular honeycomb gas seals using three different friction-factor models. *J. Trib.*, 124(3):524–529, 2002.

[11] F Ehrich. Aeroelastic instability in labyrinth seals. 1968.

[12] Dursun Eser and Jacob Y Kazakia. Air flow in cavities of labyrinth seals. *International Journal of Engineering Science*, 33(15):2309–2326, 1995.

[13] Marine Fleury. *Étude expérimentale d'instabilités aéroélastiques de joints labyrinthes*. PhD thesis, Université de Lyon, 2021.

[14] Maksim Isidorovich Gurevich. *The theory of jets in an ideal fluid*. Elsevier, 2014.

[15] Takuzo Iwatsubo. Evaluation of instability forces of labyrinth seals in turbines or compressors. *NASA. Lewis Res. Center Rotordyn. Instability Probl. in High-Performance Turbomachinery p139-167 (SEE N80-29706 20-37)*, 1980.

[16] Takuzo Iwatsubo, Naoto Motooka, and Roji Kawai. Flow induced force of labyrinth seal. *NASA. Lewis Research Center Rotordyn. Instability Probl. in High-Performance Tubomachinery*, 1982.

[17] Artur Szymański and Sławomir Dykas. Evaluation of leakage through labyrinth seals with analytical models. *TASK Quarterly. Scientific Bulletin of Academic Computer Centre in Gdansk*, 23(1):61–73, 2014.

DOI: 10.13009/EUCASS2023-650

[18] Almudena Vega and Roque Corral. Conceptual flutter analysis of labyrinth seals using analytical modelsâpart ii: Physical interpretation. *Journal of Turbomachinery*, 140(12):121007, 2018.

[19] Nicole Zirkelback and Luis San Andres. Bulk-flow model for the transition to turbulence regime in annular pressure seals. *Tribology transactions*, 39(4):835–842, 1996.

Appendices

A. Axial mass flow rate definition

By definition, cavity inlet and outlet mass flow rate respectively correspond to:

$$\begin{aligned} Q_i &= \rho_{i-1} V_{i-1} B_{z_1} \\ Q_{i+1} &= \rho_i V_i B_{z_2} \end{aligned} \tag{41}$$

where B_{z_1} and B_{z_2} are the cavity sections crossed by the flow in correspondence of the first and the second tooth.
In the case of an axisymmetric system, a more practical definition of axial mass flow rate can be obtained by normalizing Q_i and Q_{i+1} by the length of a generic circular arc of amplitude $d\theta$:

$$\begin{aligned} \dot{m}_i &= \frac{Q_i}{R_s d\theta} = \rho_{i-1} V_{i-1} \frac{B_{z_1}}{R_s d\theta} = \rho_{i-1} V_{i-1} \bar{B}_{z_1} \\ \dot{m}_{i+1} &= \frac{Q_{i+1}}{R_s d\theta} = \rho_i V_i \frac{B_{z_2}}{R_s d\theta} = \rho_i V_i \bar{B}_{z_2} \end{aligned} \tag{42}$$

where:

$$\begin{aligned} \bar{B}_{z_1} &= \frac{1}{2R_s} h_{z_1} \left[h_{z_1} + 2\left(R_s + h_t\right) \right] \\ \bar{B}_{z_2} &= \frac{1}{2R_s} h_{z_2} \left[h_{z_2} + 2\left(R_s + h_t\right) \right] \end{aligned} \tag{43}$$

B. Rotor and stator non-dimensional coefficients

Definition of the non-dimensional coefficients a_r and a_s, taking into account the length of the contact between the flow and rotor/stator wall in shear stress work:

- for tooth on rotor (TOR) configuration:
  $a_s = 1,\ a_r = (2B_i + L_i)/L_i$
- for tooth on stator (TOS) configuration:
  $a_s = (2B_i + L_i)/L_i,\ a_r = 1$

C. First-order fluid equations

Linearised formulation of first-order fluid equations.

- Continuity equation:

$$\frac{A_{0,i}}{R_g T_{0,i}} \frac{\partial P_{1,i}}{\partial t} + \frac{P_{0,i}}{R_g T_{0,i}} \frac{\partial A_{1,i}}{\partial t} - \frac{P_{0,i}}{R_g T_{0,i}^2} \frac{\partial T_{1,i}}{\partial t} + \frac{1}{R_s} \frac{U_{0,i} A_{0,i}}{R_g T_{0,i}} \frac{\partial P_{1,i}}{\partial \theta} + \frac{1}{R_s} \frac{P_{0,i} A_{0,i}}{R_g T_{0,i}} \frac{\partial U_{1,i}}{\partial \theta} + \frac{1}{R_s} \frac{P_{0,i} U_{0,i}}{R_g T_{0,i}} \frac{\partial A_{1,i}}{\partial \theta} - \frac{1}{R_s} \frac{P_{0,i} U_{0,i}}{R_g T_{0,i}^2} \frac{\partial T_{1,i}}{\partial \theta}$$
$$= \dot{m}_{1,i} - \dot{m}_{1,i+1}$$

$$\Rightarrow G_{1,i} \frac{\partial P_{1,i}}{\partial t} + G_{2,i} \frac{\partial A_{1,i}}{\partial t} + G_{3,i} \frac{\partial T_{1,i}}{\partial t} + \frac{U_{0,i}}{R_s} G_{1,i} \frac{\partial P_{1,i}}{\partial \theta} + \frac{P_{0,i}}{R_s} G_{1,i} \frac{\partial U_{1,i}}{\partial \theta} + \frac{U_{0,i}}{R_s} G_{2,i} \frac{\partial A_{1,i}}{\partial \theta} + \frac{U_{0,i}}{R_s} G_{3,i} \frac{\partial T_{1,i}}{\partial \theta}$$
$$+ G_{4,i} P_{1,i} + G_{5,i} P_{1,i-1} + G_{6,i} P_{1,i+1} + G_{7,i} T_{1,i+1} + G_{8,i} T_{1,i} + G_{9,i} h_{1,i} + G_{10,i} h_{1,i+1} = 0$$

DOI: 10.13009/EUCASS2023-650

where:

$$
\begin{aligned}
G_{1,i} &= \frac{A_{0,i}}{R_g T_{0,i}} & G_{6,i} &= \dot{m}_{0,i} C^{\dot{m}}_{0,i+1} \\
G_{2,i} &= \frac{P_{0,i}}{R_g T_{0,i}} & G_{7,i} &= D^{\dot{m}}_{0,i+1} \\
G_{3,i} &= -\frac{P_{0,i} A_{0,i}}{R_g T^2_{0,i}} & G_{8,i} &= -D^{\dot{m}}_{0,i} \\
G_{4,i} &= \dot{m}_{0,i}(B^{\dot{m}}_{0,i+1} - C^{\dot{m}}_{0,i}) & G_{9,i} &= A^{\dot{m}}_{0,i} \\
G_{5,i} &= -\dot{m}_{0,i} B^{\dot{m}}_{0,i} & G_{10,i} &= A^{\dot{m}}_{0,i+1}
\end{aligned}
$$

- Momentum equation:

$$
\frac{P_{0,i} A_{0,i}}{R_g T_{0,i}} \frac{\partial U_{1,i}}{\partial t} + \frac{P_{0,i} A_{0,i} U_{0,i}}{R_s R_g T_{0,i}} \frac{\partial U_{1,i}}{\partial \theta} + \frac{A_{0,i}}{R_s} \frac{\partial P_{1,i}}{\partial \theta} + \dot{m}_{0,i+1} U_{1,i} - \dot{m}_{0,i} U_{1,i-1} + \dot{m}_{1,i}(U_{0,i} - U_{0,i-1}) - \tau_{r_{1,i}} a_r L + \tau_{s_{1,i}} a_s L = 0
$$

$$
\Rightarrow X_{1,i} \frac{\partial U_{1,i}}{\partial t} + \frac{U_{0,i}}{R_s} X_{1,i} \frac{\partial U_{1,i}}{\partial \theta} + \frac{A_{0,i}}{R_s} \frac{\partial P_{1,i}}{\partial \theta} + X_{2,i}(U_{1,i} - U_{1,i-1}) + X_{3,i} P_{1,i} + X_{4,i} P_{1,i-1} + X_{5,i} h_{1,i} + X_{6,i} T_{1,i} = 0
$$

$$
\begin{aligned}
X_{1,i} &= \frac{P_{0,i} A_{0,i}}{R_g T_{0,i}} & X_{4,i} &= \dot{m}_{0,i+1} \left(U_{0,i} - U_{0,i-1}\right) B^{\dot{m}}_i \\
X_{2,i} &= \dot{m}_{0,i+1} & X_{5,i} &= \dot{m}_{0,i} \left(U_{0,i} - U_{0,i-1}\right) A^{\dot{m}}_i \\
X_{3,i} &= \dot{m}_{0,i} \left(U_{0,i} - U_{0,i-1}\right) C^{\dot{m}}_i & X_{6,i} &= \dot{m}_{0,i} \left(U_{0,i} - U_{0,i-1}\right) D^{\dot{m}}_i
\end{aligned}
$$

- Energy equation:

$$
\frac{\gamma - 1}{\gamma P_{0,i}} T_{0,i} P_{1,i} - T_{1,i} = 0 \tag{44}
$$

Coefficients $A^{\dot{m}}, B^{\dot{m}}, C^{\dot{m}}, D^{\dot{m}}$ derive from the linearisation of axial mass-flow , so they can have different formulations according to the assumed models for $\dot{m}$.

$$
\begin{aligned}
\dot{m}_{1,i} &= \left[\frac{\partial \dot{m}_{1,i}}{\partial h_{1,z_1}}\right]_{h_{0,i}} h_{1,z_1} + \left[\frac{\partial \dot{m}_{1,i}}{\partial P_{1,i-1}}\right]_{P_{0,i-1}} P_{1,i-1} + \left[\frac{\partial \dot{m}_{1,i}}{\partial P_{1,i}}\right]_{P_{0,i}} P_{1,i} + \left[\frac{\partial \dot{m}_{1,i}}{\partial T_{1,i}}\right]_{T_{0,i}} T_{1,i} \\
&= A^{\dot{m}}_{0,i} h_{1,z_1} + B^{\dot{m}}_{0,i} P_{1,i-1} + C^{\dot{m}}_{0,i} P_{1,i} + D^{\dot{m}}_{0,i} T_{1,i}
\end{aligned}
$$

$$
\begin{aligned}
\dot{m}_{1,i+1} &= \left[\frac{\partial \dot{m}_{1,i+1}}{\partial h_{1,z_2}}\right]_{h_{0,z_2}} h_{1,z_2} + \left[\frac{\partial \dot{m}_{1,i+1}}{\partial P_{1,i}}\right]_{P_{0,i}} P_{1,i} + \left[\frac{\partial \dot{m}_{1,i+1}}{\partial P_{1,i+1}}\right]_{P_{0,i+1}} P_{1,i+1} + \left[\frac{\partial \dot{m}_{1,i+1}}{\partial T_{1,i+1}}\right]_{T_{0,i+1}} T_{1,i+1} \\
&= A^{\dot{m}}_{0,i+1} h_{1,z_2} + B^{\dot{m}}_{0,i+1} P_{1,i} + C^{\dot{m}}_{0,i+1} P_{1,i+1} + D^{\dot{m}}_{0,i+1} T_{1,i+1}
\end{aligned}
$$